Abl signaling directs growth of a pioneer axon in *Drosophila* by shaping the intrinsic fluctuations of actin

Akanni Clarke[a,b], Philip G. McQueen[c], Hsiao Yu Fang[a], Ramakrishnan Kannan[a,†], Victor Wang[c,‡], Evan McCreedy[c], Stephen Wincovitch[d], and Edward Giniger[a,*]

[a]National Institute of Neurological Disorders and Stroke, [c]Center for Information Technology, and [d]National Human Genome Research Institute, National Institutes of Health, Bethesda, MD 20892; [b]Department of Biochemistry and Molecular Medicine, George Washington University School of Medicine/National Institutes of Health Graduate Partnerships Program, Washington, DC 20037

ABSTRACT **The fundamental problem in axon growth and guidance is understanding how cytoplasmic signaling modulates the cytoskeleton to produce directed growth cone motility. Live imaging of the TSM1 axon of the developing *Drosophila* wing has shown that the essential role of the core guidance signaling molecule, Abelson (Abl) tyrosine kinase, is to modulate the organization and spatial localization of actin in the advancing growth cone. Here, we dissect in detail the properties of that actin organization and its consequences for growth cone morphogenesis and motility. We show that advance of the actin mass in the distal axon drives the forward motion of the dynamic filopodial domain that defines the growth cone. We further show that Abl regulates both the width of the actin mass and its internal organization, spatially biasing the intrinsic fluctuations of actin to achieve net advance of the actin, and thus of the dynamic filopodial domain of the growth cone, while maintaining the essential coherence of the actin mass itself. These data suggest a model whereby guidance signaling systematically shapes the intrinsic, stochastic fluctuations of actin in the growth cone to produce axon growth and guidance.**

Monitoring Editor
Richard Fehon
University of Chicago

Received: Oct 11, 2019
Revised: Dec 19, 2019
Accepted: Jan 14, 2020

INTRODUCTION

The core challenge in axon growth and guidance is to dissect how directed motility of the growth cone arises from the action of cytoplasmic signaling molecules in response to external cues. On the basis of studies of neurons in vitro, for many years we have focused on deterministic models of clutch-like machines thought to generate forward motion by linking actin flow in a leading lamella to the fulcrum provided by adhesive junctions formed to a rigid, underlying substratum (Suter and Forscher, 2000).

In the accompanying paper (Clarke *et al.*, 2020), however, we have shown that a pioneer axon of *Drosophila*, TSM1, like many pioneer axons in the compliant medium of developing tissue, advances in a mode that appears to be fundamentally different: a protrusive mode of growth dependent on selective stabilization of a subset of appropriately oriented projections and disassembly of nonselected projections. It is quite unclear how, and whether, the familiar adhesive mechanisms would apply to this very different machine.

In recent years, it has come to be appreciated that cytoskeletal dynamics in general, and motility in particular, are in their essence stochastic processes with a high level of variability, most notably for single-cell processes, such as the advance of single growth cones (Kulkarni *et al.*, 2013; Padmanabhan and Goodhill, 2018; Bagonis *et al.*, 2019). It has been shown that fluctuation, variation, noise, and the averaging of information in time and space are of the essence of single-cell morphogenetic mechanisms, as they allow efficient and

This article was published online ahead of print in MBoC in Press (http://www.molbiolcell.org/cgi/doi/10.1091/mbc.E19-10-0564) on January 22, 2020.

Author contributions: Experimental design: A.C., P.G.M., H.Y.F., R.K., S.W., and E.G.; experiment performance: A.C. and S.W.; data analysis: A.C., P.G.M., H.Y.F., T.B., E.J., and E.G.; preparation of text and images: A.C., P.G.M., and E.G.; other: software development: A.C., P.G.M., V.W., E.M., and E.J.

Present addresses: †Department of Neurology, Yale University School of Medicine, New Haven, CT 06519; ‡The Jackson Laboratory for Genomic Medicine, Farmington, CT 06032.

*Address correspondence to: Edward Giniger (ginigere@ninds.nih.gov). ORCID: 0000-0002-8340-6158.

Abbreviations used: Abl, Abelson; CM, culture media; FI, Fisher Information Content; JSD, Jensen–Shannon divergence; KD, knockdown; LatB, latrunculin B; OE, overexpression; PCA, principal component analysis.

reliable extraction of information even in the context of the extremely low signal-to-noise that is often found, for example, in gradients of biological signals in the complex milieu of a developing animal (Cohen *et al.*, 2010; He *et al.*, 2010). In the context of directed motility, for example, this has been worked out most rigorously in bacterial chemotaxis, in which guidance arises as a "random walk with a ratchet," that is, by the imposition of a very modest, spatially oriented, statistical bias onto the probability of a biochemical process that is inherently stochastic (Macnab and Koshland, 1972; Wadhams and Armitage, 2004).

This view, together with the results of the accompanying paper (Clarke *et al.*, 2020), reveals that any serious analysis of the mechanism of axon growth and guidance must be grounded in the biophysics of the actin network of the growth cone: its distribution, organization, and dynamics. With this in mind, we reasoned that the key to ascertaining the mechanism of TSM1 growth and guidance was to use high-resolution live imaging to monitor in real time the actin cytoskeleton of the advancing growth cone as we manipulate experimentally a cytoplasmic signaling module that implements axon growth and guidance signals, the Abelson (Abl) tyrosine kinase. This is a signaling network whose loss-of-function often causes axon stalling, while its overactivation can cause axon misrouting (Wills *et al.*, 1999a,b; Crowner *et al.*, 2003; see also the accompanying paper, Clarke *et al.*, 2020, Supplemental Figure S4)

In the current work, we show that Abl tyrosine kinase regulates the organization and redistribution of an accumulated actin bolus in the growth cone that directs the extension and guidance of the TSM1 axon by regulating the spatial localization of filopodial morphogenesis. Specifically, the distal portion of the TSM1 axon accumulates a bolus of actin that displays forward-biased spatial fluctuations, leading over time to its net advance during axon growth. Advance of the actin bolus, in turn, locally enhances the density of filopodial protrusions in the region where actin moves to and allows the disassembly of protrusions in its wake, resulting in progressive advance of the filopodia-rich domain that defines the growth cone morphologically. The redistribution of actin is itself coordinated by the Abl tyrosine kinase signaling pathway, which dynamically modulates the spatial width of the actin distribution and also minimizes its disorder, allowing predictable translocation of the growth cone. Together, these data show how Abl probabilistically shapes the propagation of a leading actin mass that directs the growth and guidance of a pioneer axon extending in its native environment.

RESULTS

Advance of the accumulated actin distribution predicts the local growth and disassembly of axonal protrusions

An extensive literature exists describing the causal role of actin in the genesis and dynamics of filopodia (Svitkina *et al.*, 2003; Lebrand *et al.*, 2004; Mogilner and Rubinstein, 2005; Goncalves-Pimentel *et al.*, 2011; Bilancia *et al.*, 2014). This, together with our observations of TSM1 in the accompanying paper (Clarke *et al.*, 2020), led us to hypothesize that advance of the actin mass found in the distal portion of the axon (referred to below as the "actin peak") drives processive axonal growth. To test this hypothesis, we first selected all wild-type trajectories in which the actin peak advanced at least 20 µm during the imaging session. We then quantified the protrusion density over time in a 10-µm interval centered on the initial position of the actin maximum (the starting position) and in a second 10-µm interval centered 20 µm further distal down the axon (Figure 1). Consistent with visual inspection of TSM1 dynamics, we found that, after a lag phase of ~15 min, the summed protrusion length declined by 50% ± 0.1 (mean ± SEM, $p < 0.001$) in the region vacated by the actin peak, while at the new more distal position of the actin peak, the protrusion length was increased by 32% ± 0.1 (mean ± SEM, $p < 0.01$) (Figure 1A). The same pattern was observed in independent data sets from two other genotypes (Abl knockdown [KD] and Abl overexpression [OE]; Figure 1, B and C). For comparison, a gallery of representative images from a single wild-type trajectory is shown in Figure 1D (see also Supplemental Figure S1 for the same images pseudocolored by actin intensity and Supplemental Video S2 of the accompanying paper [Clarke *et al.*, 2020] for the complete movie of this trajectory). Thus, displacement of the actin distribution predicts axon consolidation where actin has vacated and growth cone expansion where actin has now accumulated. In this way, advance of accumulated actin advances the growth cone and extends the TSM1 axon.

The above data suggest that the anterograde displacement of the actin peak occurs before changes in growth cone morphology and extension of the axon. If this is true, on average we would expect to find the actin peak further distal along the axon in individual time points than is the peak density of growth cone protrusions. To test this prediction, we aligned all 338 wild-type time points by the protrusion maximum along the axon and plotted the position of the actin maximum, as well as the positions of the proximal and distal boundaries of the actin peak. Empirically, we found it effective to define the boundaries of the actin peak by the leading and trailing square root of the second moment of the actin distribution about the actin maximum (a measure akin to the SD of the distribution; see below and *Materials and Methods* of the accompanying paper [Clarke *et al.*, 2020] for a detailed discussion of the rationale behind this definition; see also Figure 4C of Clarke *et al.* [2020] for an illustration). We found that the average position of the actin maximum led the maximum of the protrusion density by an offset distance of 2.8 µm ± 0.58, (mean ± SEM, $p < 0.0001$), with the actin peak as a whole enveloping the position of maximum protrusion density (Figure 1E). Since the TSM1 axon grows at an average rate of 0.23 µm/min (as measured by a variety of metrics; see Supplemental Figure S2), this mean offset length implies that the position of the actin maximum predicts where the maximum of protrusions will be found 10–15 min later (corresponding to 3–5 time points later in our imaging), consistent with the lag observed above in individual instances of growth cone advance. Similarly, the actin peak was also found to lead the protrusion peak if we used the midpoints rather than the maxima of the two distributions as the reference point, or if we used a method employing the entire actin and protrusion distributions, rather than any single fiducial point, for the comparison. Finally, the offset distance between the actin maximum and that of the protrusion density appears to be maintained actively. We found a strong negative correlation between the rate of change of the offset distance between these two positions in pairs of successive time points ($r = –0.50$, $p < 0.0001$) (Figure 1F), which suggests that when the spacing between the actin and protrusion maxima increases or decreases in any given time step, the gap size tends to be restored during the next time point. Taken together, these data suggest that advance of the actin peak drives axon growth by directing the site of growth cone protrusion, with the offset distance between these two axonal features being a regulated aspect of axon growth.

Net forward motion of the actin distribution arises from biased, stochastic fluctuations of the distribution

In light of the observation that the shape of the actin distribution is the target of guidance signaling downstream of Abl, and that the pattern of actin redistribution predicts where axonal protrusions will retract and grow, we next examined the evolution of the actin distribution itself over time in each trajectory. We found that anterograde

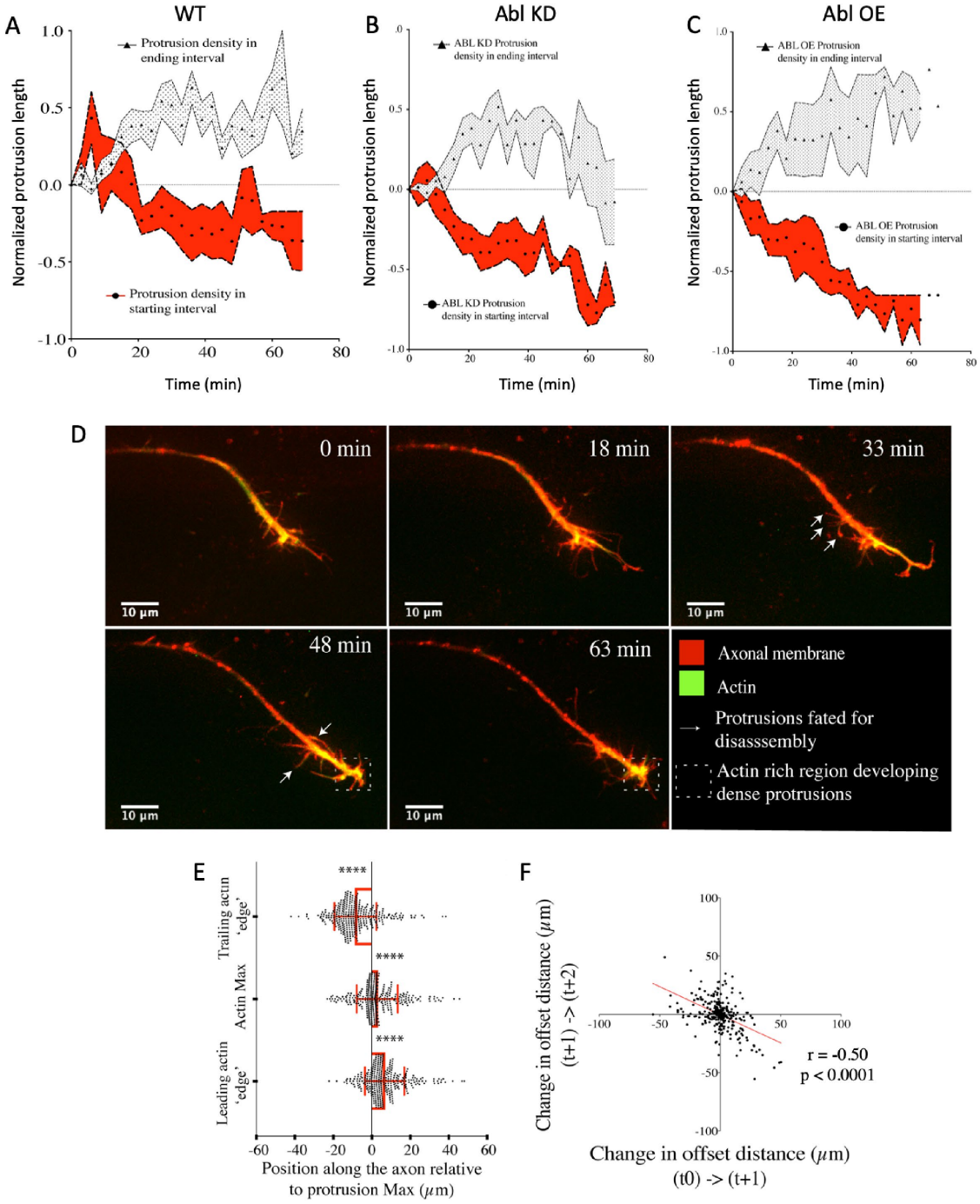

FIGURE 1: Actin leads and predicts the advance of the axonal protrusion density. (A–C) Trajectories that achieved 20 µm of actin advance were aligned by the midpoint of the actin distribution at the start of that advance. Average protrusion length over time is plotted for a 10-µm interval centered on the midpoint of the actin distribution at the start of the actin translocation events (red and black checkered swath), and for the interval centered 20 µm distal to that start point (black and white swath). Protrusion length for each 20-µm actin midpoint translocation event analyzed was normalized to the summed protrusion length at $t = 0$; $n = 128$ time points from seven individual trajectories; mean ± SEM for each time point is plotted over time. (A) Wild type, (B) Abl KD, (C) Abl OE. (D) Gallery of images showing time course of TSM1 axon extension and actin advance (lifeact-GFP, green; and CD4 tandem tomato, red). White arrows highlight protrusions that disassemble over time as actin advances; dashed white box highlights protrusions formed in domain of high actin density. (E) The maximum of the actin distribution, as well as the leading and trailing "edges" of the distributions are plotted relative to the position of the maximum protrusion density along the axon, which is set at the origin. Significance of the offset of these actin landmark positions relative to protrusion density in each respective time point was determined by two-tailed paired t test; $n = 338$ time points from 14 individual trajectories, ****$p < 0.0001$). (F) A scatter plot of the change in the offset distance between actin and protrusion maxima in one time step vs. the change in the offset distance in the preceding time step; $n = 338$ time points from 14 individual trajectories; Pearson r.

translocation of the actin peak was not constant. Rather, both the maximum of the actin peak and its midpoint displayed extensive, seemingly stochastic fluctuations proximodistally along the axon, but with a small anterograde bias that resulted, over time, in net forward motion of the actin peak (Figure 2A). This bias in the stochastic motion of these positions is evident upon tracking the positions of the front, rear, and maximum of the actin distribution over time for any single trajectory (Figure 2A), or by plotting a histogram of the translocations of the actin maximum (Figure 2B). Further inspection of actin redistribution patterns revealed that the position of the actin maximum largely fluctuates at each time step within the domain defined as the actin peak (i.e., the window defined by the leading and trailing square root of the second moment of the actin peak; 77% of time steps in wild type [251/327]). Consistent with this, we found that a broader actin peak allowed larger excursions of the maximum and midpoint, while narrow actin peaks were correlated with relatively short fluctuations of the position of the actin maximum (Pearson $r = 0.24$, $p < 0.0001$) (Figure 2C). Thus, the net effect of the actin fluctuations is that the actin distribution displays an "inchworm" style of motion, with the front of the actin peak advancing over time and the rear catching up. This can also be seen, for example, in Figure 2F of the accompanying paper (Clarke *et al.,* 2020).

Our consistent observation of inchworm-like fluctuations of the actin distribution during processive TSM1 growth cone advance in all genotypes led us to hypothesize that these fluctuations are central to the mechanism of axonal growth. To test this hypothesis, we suppressed actin dynamics by applying latrunculin B (LatB) to wing explant cultures 5 min before the start of TSM1 imaging. Lat B significantly decreased the magnitude of displacements of the actin maximum ($p < 0.05$, KS test, $n = 125$ time points [control], 123 [LatB]) (Figure 2D) and greatly reduced TSM1 growth rate as compared with the vehicle control (–0.0030 μm/min ± 0.12 in LatB vs. 0.37 μm/min ± 0.07 in dimethyl sulfoxide [DMSO] control; mean ± SEM, $p = 0.024$ unpaired *t* test, $n = 7$ LatB trajectories and 8 DMSO trajectories) (Figure 2E). These data further support the hypothesis that spatial fluctuations of the distribution of actin are a key mechanistic component of TSM1 growth.

Actin accumulation is fragmented and advance of the distribution is unpredictable in Abl-perturbed backgrounds

The most striking consequence of Abl deregulation in individual images is fragmentation of the actin distribution (Figure 3, A–D). We quantified this phenotype using a measure from information theory called the Fisher Information Content (FI), which measures the "roughness" of the actin distribution, including, for example, both short-range fluctuations of intensity (<1 μm spatial scale) and mid- to long-range "clumping" of actin (2–20 μm scale). We find that the actin distribution profiles from Abl-perturbed axons are vastly fragmented as compared with controls (3.87 ± 0.14 in control vs. 32.67 ± 1.76 in Abl KD and 18.54 ± 1.40 in Abl OE; mean ± SEM, $p < 0.001$ in each comparison) This suggests that one effect of Abl is to regulate the coherence of the actin distribution in the axon at any single time point.

Next, we compared the actin distribution dynamics in the wild-type condition with the Abl-perturbed conditions and found that the actin distribution evolves in an orderly way from one time step to the next in wild type, but much less so when Abl is dysregulated (Figure 3, E–H′, and Supplemental Videos S1–S3). The evolution of the actin distribution was quantified using another approach from information theory, called the Jensen–Shannon divergence (JSD), which calculates the dissimilarity ("divergence") of the shape of the actin distribution between pairs of time points in a given trajectory. Thus, two distributions that are very similar have very low divergence (JSD close to 0), while two distributions that are very different have high divergence (JSD close to 1). In the control condition, successive time points of any single trajectory tended to have highly overlapped distributions, and thus low JSD values, and the overlap tended to decay in an orderly way as comparisons were made to more distant time points (Figure 3, F and F′). In contrast, in the Abl KD and Abl OE conditions, the overlap between nearest neighbor time points was commonly as dissimilar as that of two distributions separated by multiple time steps in the wild-type condition, as indicated by increased mean JSD values (0.17 ± 0.0039 in the control vs. 0.38 ± 0.011 in the KD and 0.29 ± 0.011 in the OE; mean ±SEM, $p < 0.001$; Figure 3, G, H, G′, and H′; the cumulative distribution of JSD values for all genotypes is presented in Supplemental Figure S3, and the videos corresponding to Figure 3, F, G, and H, are presented as Supplemental Videos S1, S2, and S3, respectively). These data demonstrate dynamic order in the temporal evolution of the actin distribution in each WT TSM1 trajectory, while in the Abl-perturbed conditions, that same evolution is dynamically disordered and unpredictable.

Actin disorganization correlates with morphological phenotypes in Abl-perturbed backgrounds

The correlation analyses and principal component analysis (PCA) in the accompanying paper (Clarke *et al.,* 2020) clearly demonstrate that Abl, the conserved mediator of signaling from many common axon guidance receptors, primarily modulates an interlinked cluster of growth cone parameters comprising actin coherence—actin fragmentation and dynamic actin instability—together with a parameter that links the actin peak back to morphology: the spatial offset between the peaks of actin accumulation and filopodial protrusion. We therefore examined in more detail the morphological correlates of the actin coherence values we have measured for TSM1. To our surprise, we found that high fragmentation of the actin distribution was associated preferentially with the shortest growth cones in Abl KD ($r = –0.14$; $p = 0.005$), but it was associated with the longest growth cones in Abl OE ($r = 0.25$; $p < 0.0001$) (Figure 4A). In the case of Abl KD, this reflected a population of very short growth cones with hypercondensed actin, that is, growth cones containing small, intensely labeled foci of actin. Data presented above showed that actin step size, that is, the distance the actin maximum (or midpoint) advances in any single time step, correlates with the length of the actin peak (Figure 2C). In Abl KD, however, the growth cone often contracts beyond the lower limit observed in wild type, and the step size falls to nearly zero (Figure 4, B and C). Consistent with this, Abl KD is a genotype in which we observe growth cone stalling and failure to form an axon (Supplemental Figure S4 of the accompanying paper [Clarke *et al.,* 2020]; see also Wills *et al.*, 1999b; Crowner *et al.*, 2003). In contrast, in Abl OE, a genotype commonly associated with axon misrouting (Supplemental Figure S4 of the accompanying paper [Clarke *et al.,* 2020]; see also Wills *et al.*, 1999a; Crowner *et al.*, 2003), maximal disruption of actin is associated preferentially with the longest actin distributions, and in particular, with distributions substantially broader than the upper limit typically observed in wild type (Figure 4, D and E). These abnormally broad distributions often greatly exceed the distance over which the motions of individual actin molecules display correlated motion within a disordered actin network (decay length ~11–16 μm; Linsmeier *et al.*, 2016), perhaps accounting for the failure of this genotype to respond faithfully to the distribution of guidance information in the substratum; in essence, the actin mass is so extended that actin behavior at the front of the growth cone becomes uncoupled from that at the rear.

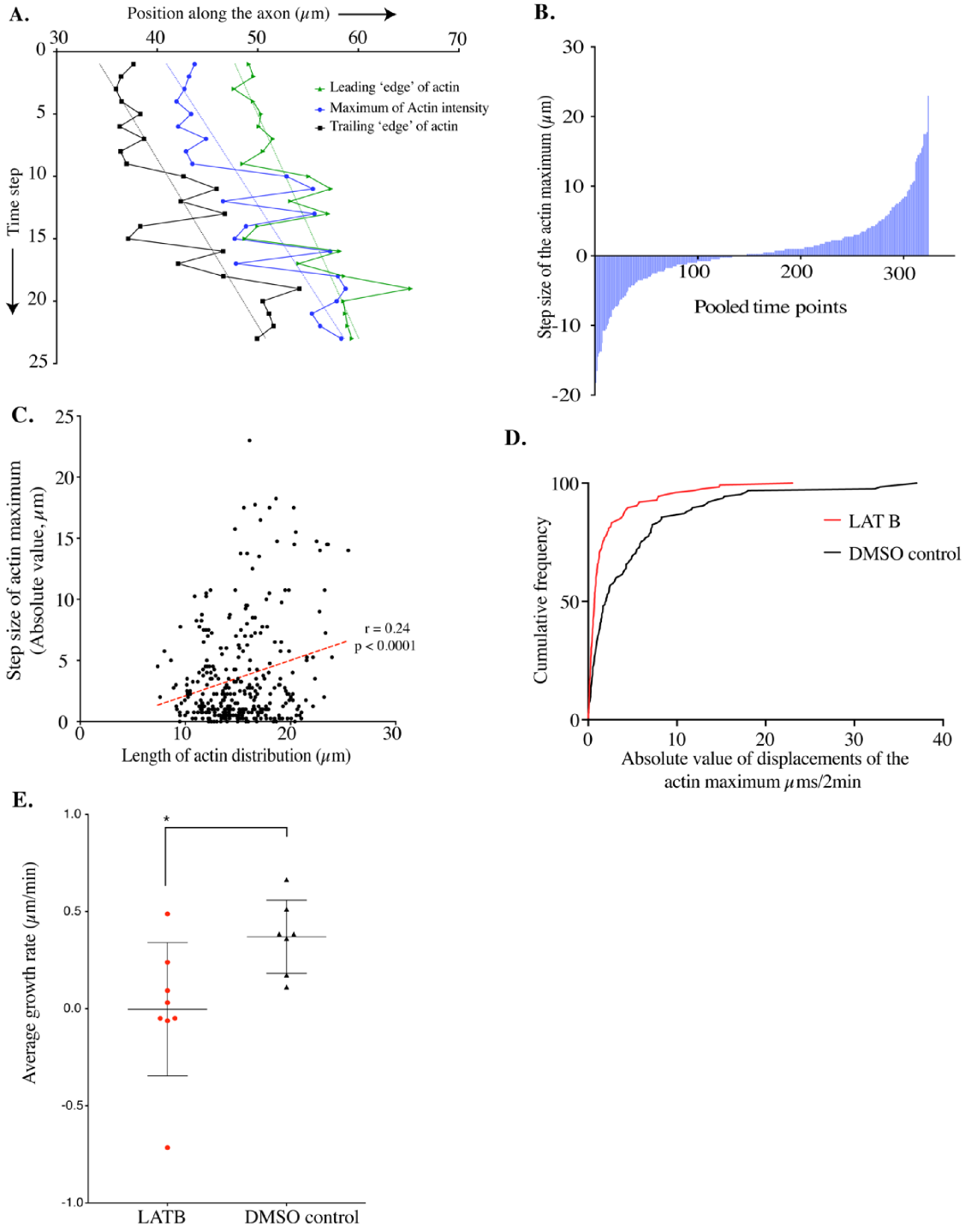

FIGURE 2: Biased stochastic fluctuations of accumulated actin move the distribution forward. (A) Plot of the axonal positions of landmarks in the actin distribution from a single trajectory over time. The actin maximum (blue) and the leading (green) and trailing (black) edges of the actin distribution are highlighted. This example is representative of $n = 14$ independent trajectories. (B) Histogram of the length of excursions of the actin maximum in single time steps; $n = 324$ time steps from 14 individual wild-type trajectories. (C) Scatter plot of the absolute value of the step size of the actin maximum vs. the length of the actin distribution; $n = 324$ time steps from 14 individual wild-type trajectories; Pearson r correlation. (D) The magnitude of displacements of the actin maximum along the axon in LatB and DMSO-treated TSM1 neurons are presented as cumulative frequency distributions; $n = 123$ time points from seven individual trajectories (LatB) and 125 time points from eight trajectories (DMSO control). (E) Average growth rate of TSM1 axons from D, exposed to LatB or DMSO control.

Given the hypothesis that increase versus decrease of Abl activity modifies actin structure at different spatial scales, and that the definitive morphological consequences of Abl arise from that spatial dichotomy, it was essential to validate this hypothesis with a more direct measure of the effect of Abl on the structure of the growth cone actin distribution at different length scales. To this end,

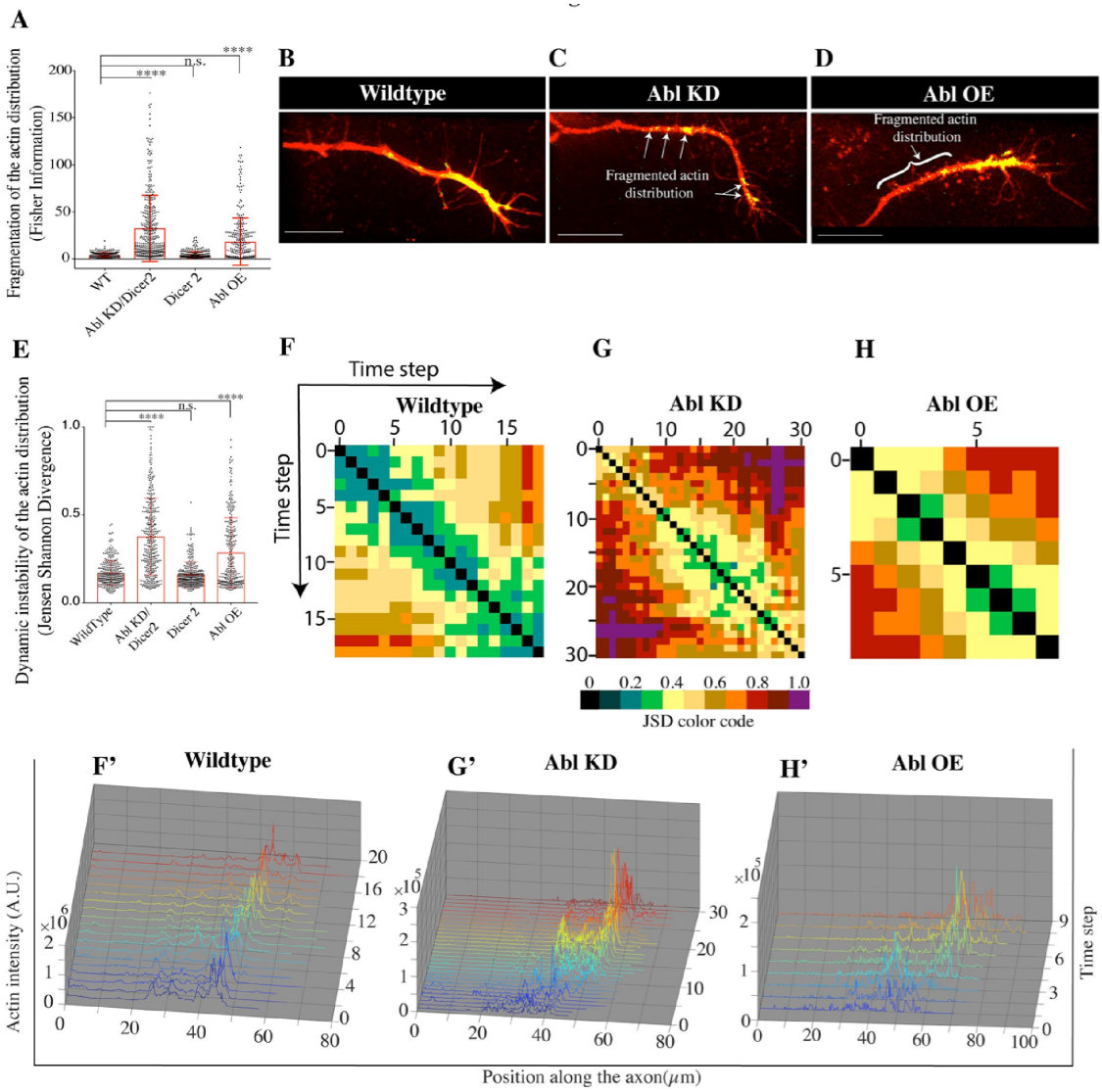

FIGURE 3: Abl perturbation fragments the actin distribution and disorganizes its advance. (A) Fragmentation of the actin distribution, as calculated by the FI of each actin profile in each time point, was quantified in the indicated genotypes. (B–D) Representative examples of the mean actin fragmentation phenotype for each genotype. Scale bar at bottom = 15 μm. (E) The dynamic instability of the actin distribution, as calculated by the JSD of sequential pairs of actin profiles over time (see *Materials and Methods*), was quantified in wild type, Abl KD, ABl OE, and in the UAS-Dicer2 control. For A and E, $n \geq 315$ time points from 14 trajectories for each genotype; significance was determined by one-way ANOVA; ****$p < 0.0001$; n.s. = nonsignificant; error bars indicate SD. (F, H) The JSD of all pairwise combinations of the actin profiles from all time steps of one individual trajectory from each genotype was calculated and color coded and are presented as matrices. The scale for the color code is shown below. In each case, the matrix shown represents a trajectory with a mean JSD value that is approximately average for that genotype. The particular Abl KD trajectory shown here (G) happens to have more time points than the wild type (F) while the Abl OE has fewer (H), but the interval between time points is the same in all cases (3 min). (F'–H') The 3D sequential actin distribution plots that correspond to the representative JSD matrices above.

the actin profile along the axon was analyzed by wavelet transformation. This method separates the contributions of different length scales to the overall pattern of actin accumulation. Consistent with the hypotheses above, when we compare the amplitudes of wavelets of different order, we found that Abl KD produces a large increase in the representation of the highest-order wavelet terms, that is, those corresponding to accumulation of clusters of dense actin foci at the smallest length scales (particularly sixth and seventh orders, corresponding to lengths <4–8 μm; Figure 5). In contrast, Abl OE selectively leads to increased representation of features on large length scales (order 4, corresponding to features in the size range of ~16–32 μm; Figure 5). These data confirm that Abl manipulations alter the spatial distribution of actin in ways that correlate with the coherence of the growth cone, such that reducing Abl activity causes condensation of actin on short spatial scales, while activating Abl produces actin expansion on a broader length scale. The potential molecular basis of these length-dependent changes in actin organization, and the mechanism by which they may account for the patterns of axon growth, will be considered in detail in the *Discussion*.

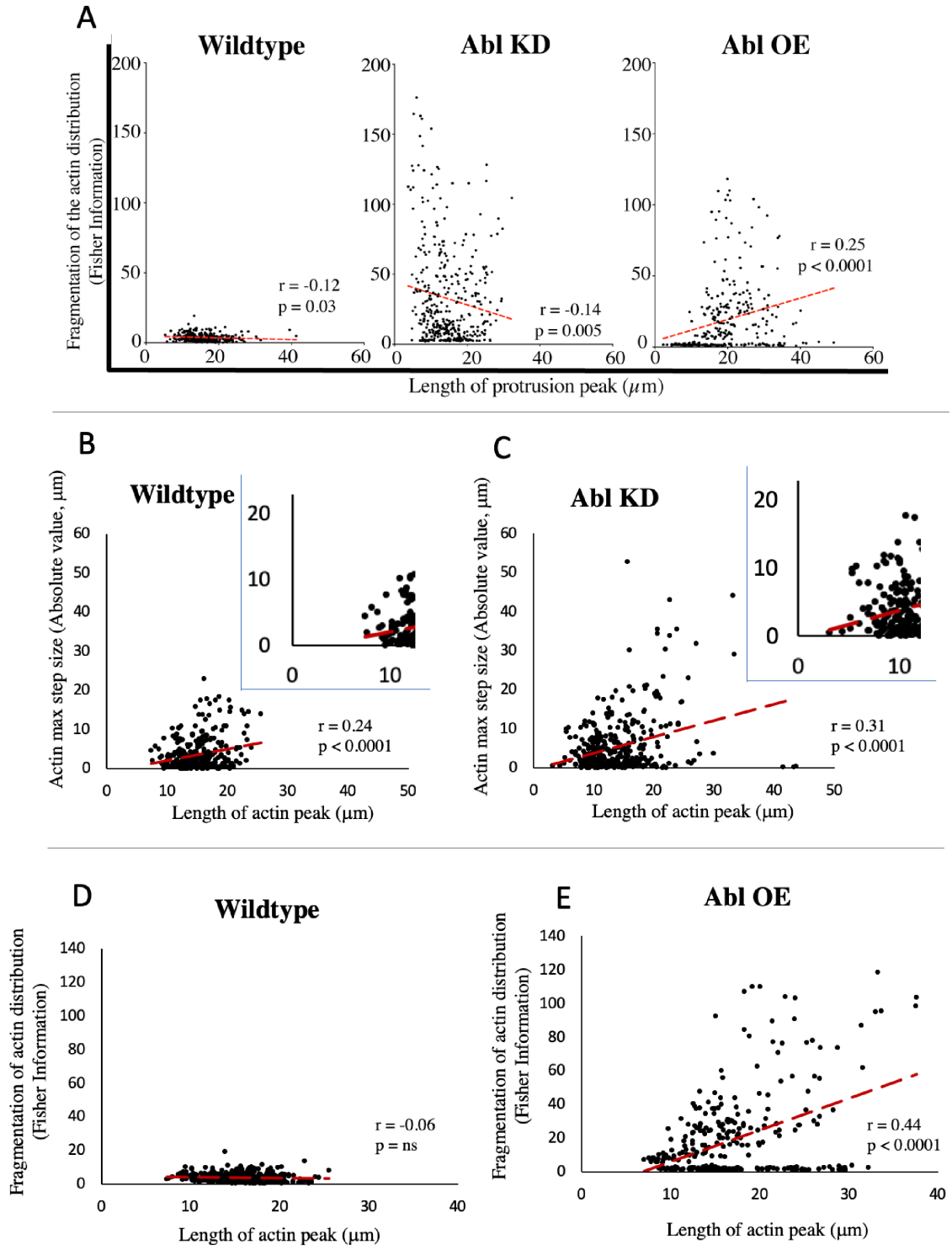

FIGURE 4: Actin fragmentation and distribution step size correlate with the length of the growth cone. (A) Scatter plot of the FI vs. the length of the protrusion peak for each indicated genotype. (B, C) Scatter plots of the absolute value of the actin peak step size vs. the length of the actin peak in wild type (B) and Abl KD (C). Insets expand the portion of the graphs near the origin. Note that very few wild-type time points have actin peak lengths <10 μm (15/324 = 4.6%), whereas in Abl KD the number <10 μm is 80/383 (20.9%), with the smallest being 3.1 μm. To facilitate comparison to the Abl KD data, B displays the same wild-type data as shown in Figure 2C. (D, E) Scatter plots of the FI vs. the length of the actin peak in wild type (D) and Abl OE (E). The actin peak lengths employed in B–E represent the sum of the leading + trailing sqrt (second moment) for each image. $n > 300$ time points from 14 individual trajectories for each genotype; Pearson r correlation.

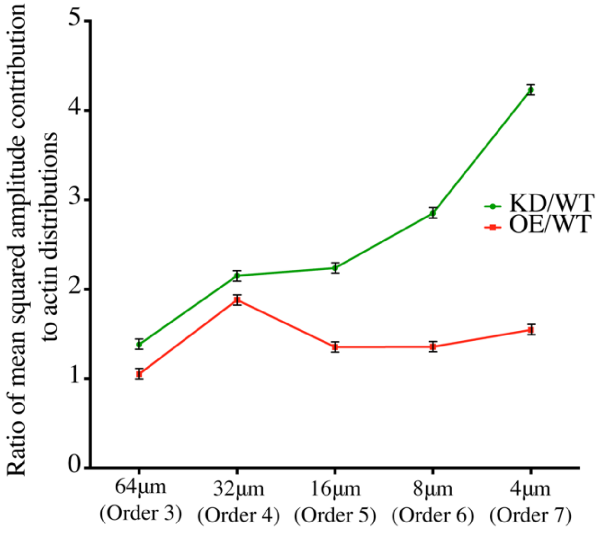

FIGURE 5: Wavelet analysis reveals the effect of Abl on the length scale of the spatial distribution of actin. Decomposition of individual actin distributions by wavelet transformation reveals the relative contribution of different length scales (orders) to the overall actin pattern in each distribution. Values reported are ratios of Abl KD or Abl OE to wild type, as indicated. Eighth and ninth order wavelet amplitudes are confounded by the spatial granularity of the image segmentation, and first and second orders reflect the residuals of the low pass filter; therefore, these are not shown. Scale at the bottom shows the approximate length scale represented by the indicated wavelet order.

DISCUSSION

What is a growth cone, and how does it extend an axon? We have shown here that a local accumulation of actin in the distal axon generates the zone of enhanced protrusive dynamics that defines the TSM1 growth cone. Over time, this actin bolus advances down the nascent axon, supporting formation of new filopodial protrusions from leading intervals now bearing enhanced actin levels, thus enabling extension of the axon. Protrusions left behind in the wake of actin advance are disassembled, thus consolidating the proximal axon. Inchworm-like dynamics advance the actin mass through an anterograde bias that moves the distribution forward over time. Furthermore, our data demonstrate that Abl tyrosine kinase, a conserved regulator of cytoskeletal dynamics that signals downstream of many guidance cue receptors, coordinates the actin fluctuations that, in aggregate, produce the net forward motion of the distribution. Taken together, our data suggest that the fundamental function of Abl during axon extension and guidance is to modulate, in a probabilistic way, the fluctuations and the coherence of the advancing actin wave that directs the construction and consolidation of the growing axon and to do so in response to guidance cues (Figure 6, A and B), as we explain below.

Axon growth and guidance occurs by directed advance of a domain of filopodial dynamics in the distal axon. In these two papers (Clarke *et al.*, 2020), however, we have shown that guidance signaling, as channeled through Abl, does not act by materially altering the morphological properties of the growth cone themselves, but rather by changing the spatial distribution of *where* those morphological properties are displayed, and that this is mediated via the Abl-dependent dynamics of actin. In particular, the PCA analysis in the accompanying paper (Clarke *et al.*, 2020) reveals that while the range of morphological states (VM2 component axis) is largely insensitive to Abl and statistically unlinked to growth cone advance, the VM1 axis is strongly Abl dependent and linked consistently to the velocity of the actin peak. This VM1 component comprises actin organization and dynamics, as well as the spatial offset between the peaks of actin and filopodia. In the current paper, we have shown that it is this offset that is the driving force for advance of the dynamic filopodial domain, which follows behind the advance of actin, both spatially and temporally. In essence, the advancing actin peak directs processive axon growth by locally promoting assembly of potential axonal tracks ahead of the growth cone, while the axon cannibalizes filopodia that lag behind the actin peak, and correspond to axonal paths that were not taken. Our observation that the actin distribution acts upstream of morphology, locally regulating filopodial extension and maintenance in growing TSM1 axons, accords well with an extensive literature in vivo, in vitro, and in silico that demonstrate the causal role of actin organization in orchestrating filopodial dynamics (Svitkina *et al.*, 2003; Lebrand *et al.*, 2004; Mogilner and Rubinstein, 2005; Goncalves-Pimentel *et al.*, 2011; Bilancia *et al.*, 2014).

Growth cone advance has often been discussed by invoking deterministic, clutch-like mechanisms that harness the adhesive properties of leading lamellipodia (Lewis and Bridgman, 1992; Lin and Forscher, 1995; Lowery and Van Vactor, 2009). For some neurons, particularly those extending axons on relatively rigid, highly adherent substrata, these models provide a plausible explanation for axon growth. However, TSM1 and many other axons are nonlamellar, particularly in compliant, 3D environments like those often encountered by pioneer axons in vivo (O'Connor *et al.*, 1990; Sabry *et al.*, 1991; Dent and Gertler, 2003; Sanchez-Soriano *et al.*, 2010). Here, growth cones are often dominated by filopodial protrusions and seem to lack the large veil-like structures that we associate with adhesive growth. Moreover, growth of these axons appears to be accomplished by protrusion and selective stabilization of filopodia, rather than by traction forces applied to the lamellipodia-like veils between filopodia (O'Connor *et al.*, 1990; Sabry *et al.*, 1991). We show here that this protrusive growth employs a mechanism that is probabilistic rather than deterministic and is based on the statistical properties of disordered actin networks in that net forward motion of the actin peak arises from a small spatial bias that is applied to the fluctuating actin distribution. These contrasting styles of axon growth are reminiscent of the dichotomy between adhesive cell motility on rigid 2D substrata versus protrusive cell motility in compliant 3D environments. They also add support to the notion that the mechanisms of motility employed by cells are not fixed, but are instead dependent on the context of their environment.

One key requirement for producing axon extension by exploiting fluctuations of the actin distribution is that the forward expansion of actin must be large enough to advance the actin bolus appreciably, yet constrained enough that the actin remains coherent and the growth cone behaves as a single, unitary entity. We see here that balancing these two competing requirements is the fundamental role of Abl tyrosine kinase. It is well established that signaling by Abl must be maintained at an intermediate level to support proper growth and guidance of axons (Koleske *et al.*, 1998; Grevengoed *et al.*, 2001; Grevengoed *et al.*, 2003; Liebl *et al.*, 2003; Moresco and Koleske, 2003). Our data indicate that this intermediate level is crucial for two reasons. First, it minimizes the disorder of the actin distribution as assayed both instantaneously by the FI of the actin profile at each time step and also dynamically by the JSD analysis of the evolution of the distribution between time steps. Second, we see

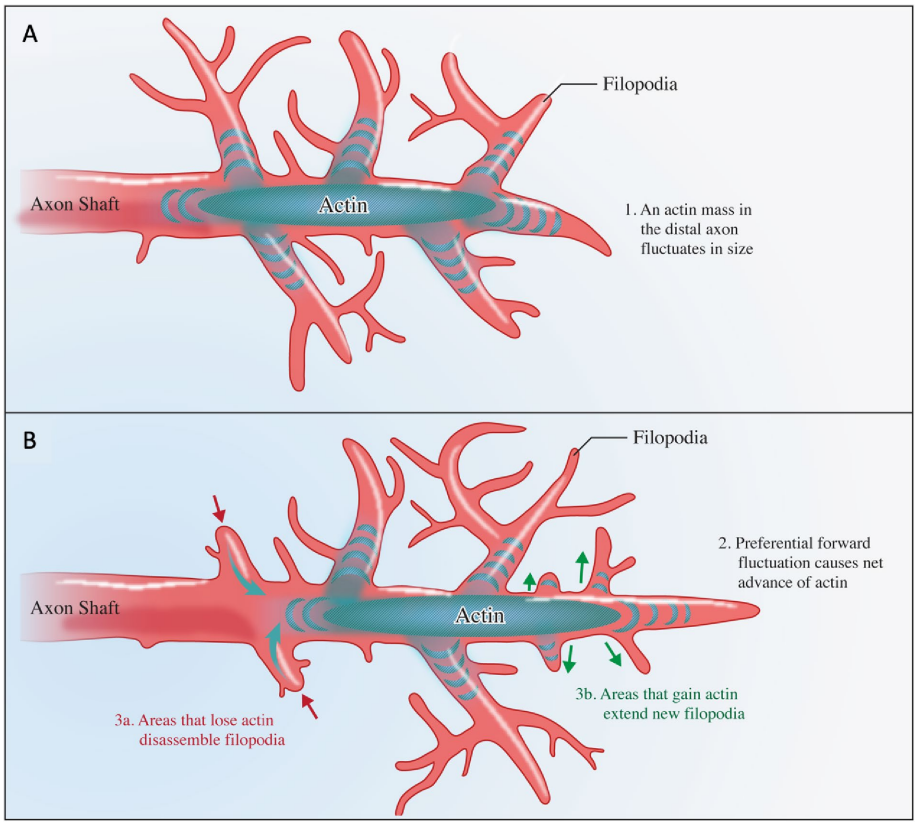

FIGURE 6: Model of actin driven axon extension and consolidation. (A, B) Models of actin-driven axon extension and consolidation. (A) Accumulated actin mass in the distal axon fluctuates in size, transiently invading growth cone protrusions. (B) Selective accumulation of actin in a more distal axonal protrusion advances the distribution and triggers the emergence of nascent protrusions in that region (green arrows), while proximal regions no longer bearing enhanced levels of accumulated actin undergo disassembly of protrusions (red arrows).

that Abl regulates the width of the actin peak. This is observed most clearly in the Abl perturbations, where reducing Abl promotes condensation of the actin mass while increasing Abl promotes expansion of the peak (Supplemental Figure S4, also see accompanying paper [Clarke *et al.*, 2020] Figure 5D). In the most severely affected time points of Abl KD and OE, these effects on peak width and actin order are likely to be responsible for the overt mutant phenotypes we observe. Abl knockdown causes the actin bolus to hypercondense and fragment into small, tightly packed foci that show reduced spatial motion (Figures 2, C–E, and 4, B and C). Since expansion of the distribution provides the forward motion required for inchworming, it is plausible that failure of that expansion in the Abl KD condition is responsible for the growth cone stalling observed in this genotype. Conversely, OE of Abl causes the actin distribution to expand excessively, often to the degree that the peak exceeds the characteristic decay length over which the motions of individual actin molecules remain correlated within disordered actin networks (~11–16 μm) (Linsmeier *et al.*, 2016). In essence, the actin peak becomes so broad that the front of the peak becomes statistically uncoupled from the back. This likely contributes to the preferential fragmentation we observe of the broadest actin peaks in the Abl OE condition (Figure 4E) and plausibly could predispose to axonal misrouting and inappropriate axon branching. The two key functions of Abl, minimizing disorder and controlling distribution width, are closely intertwined; in the Abl KD condition, the tendency is for the smallest growth cones to drive measures of disorder, while in Abl OE, it is the broader growth cones that preferentially show signatures of disorder (Figure 4, A, D, and E). Note that these data also reveal that while decrease and increase of Abl both cause disruption of the actin distribution (increase in FI and JSD), they do so in opposite ways, with Abl KD causing overrepresentation of short-range actin concentrations and Abl OE causing broad separations of actin masses (Figures 4, B–E, and 5).

Our model of growth cone behavior is derived partly from vigorous perturbations of Abl, but our goal is to understand the modest modulation of Abl by guidance receptors. The correlation and PCA studies in the accompanying paper (Clarke *et al.*, 2020, Figures 6 and 7), however, demonstrate that the relationships among actin and morphological parameters in the Abl-manipulated contexts are a faithful mirror of those relationships in wild type; they display the same morphological properties, but are subject to a quantitatively exaggerated intensity of actin inputs. Therefore, we infer that the modest decreases and increases of Abl activity produced by guidance receptors in wild-type development modulate actin condensation and expansion similarly to what we see experimentally, albeit to a more measured extent. Hence, we would predict, for example, that a guidance cue that enhances Abl activity, such as Netrin acting through DCC/Frazzled (Forsthoefel *et al.*, 2005; O'Donnell and Bashaw, 2013), would promote expansion of the actin domain, and thus bias growth, in the direction of greater cue concentration, while local accumulation of a cue that leads to reduced Abl activity, such as Delta acting through the receptor Notch (Crowner *et al.*, 2003; Kuzina *et al.*, 2011; Kannan *et al.*, 2018), would locally promote condensation of the actin and therefore focus future proliferation of filopodia from the vicinity of that accumulation. Similarly, by this model it is straightforward to see why the subcellular localization that has been observed for some guidance receptors within subregions of the growth cone (Pignata *et al.*, 2019) might be essential for them to promote either axon extension or retraction, respectively, or how a single receptor could be switched between attraction and repulsion simply by changing the polarity of its distribution in the growth cone.

A crucial mechanistic question raised by our experiments is how varying the level of Abl activity produces changes in the length of the actin peak. We have shown recently that the structure of the Abl signaling network intrinsically causes it to modulate the ratio of linear versus branched actin within the cell (Kannan *et al.*, 2017). Thus, activating Abl suppresses Enabled, a factor that extends linear actin, but stimulates the Trio, Rac1, WAVE/SCAR, Arp2,3 axis that leads to actin branching. Suppressing Abl activity has the opposite pair of effects. Remarkably, recent studies have demonstrated that simply altering the ratio of linear versus branched actin in a disordered network is sufficient to alter network dimensions in just the way we observe in TSM1(Lenz, 2014; Ennomani *et al.*, 2016; Linsmeier *et al.*, 2016). Thus, manipulations that increase the proportion of unbranched, linear actin in a moderately cross-linked actin network

favor coalescence of the distribution, while those that produce increased network cross-linking, such as a higher proportion of branched actin, tend to expand the network. These consequences of actin network modulation are consistent with the data presented here, which show that the Abl KD condition (which increases Ena activity) causes growth cones with short, hypercondensed actin distributions to be overrepresented, while in the Abl OE condition (which increases activity of Rac/WAVE), growth cones with longer, extended actin distributions are overrepresented (Figure 5 and Supplemental Figure S4; see also Figure 5C of the accompanying paper [Clarke *et al.,* 2020]). Preliminary computational simulations in our lab further support this view and suggest detailed molecular mechanisms to account for the source of these effects (A. Chandrasekaran, G. Papoian, and E.G., unpublished observations). Therefore, it is possible that the effects of Abl on the actin distribution, and thus on morphological growth and guidance, could be accounted for simply by the demonstrated biochemical effects of Abl on pathways leading to branched versus linear actin. This conjecture will be investigated experimentally in future studies, particularly by imaging TSM1 as we modify the activity of Ena and Rac.

It is well established that Abl has other roles aside from regulating actin extension and branching, such as regulation of the microtubule plus-end tracking protein Orbit (Lee *et al.*, 2004). Our data do not exclude, for example, the idea that Abl-dependent interactions of actin with microtubules could contribute to the forward bias of actin fluctuations. Moreover, in this analysis, we have tracked the bulk distribution of actin. The motions of individual actin molecules remain unknown. Evolution of the actin distribution presumably incorporates actin polymerization, branching, cross-linking, diffusion, myosin contractility, active transport, and bulk flow of actin, among others. Future experiments will aim to separate the individual contributions of these processes.

The mechanism of axon growth we observe here is energetically expensive, with only ~5–15% of the total back-and-forth motion of the actin peak being captured in net advance of the actin mass. This mechanism, however, allows extremely efficient use of guidance information. The fluctuations of the actin peak cause it to repetitively sample leading and trailing positions along the axon many times before moving irrevocably along its trajectory. Thus, any single large-scale displacement of the actin peak typically integrates a minimum of 40–60 min of back-and-forth fluctuations (Figure 2, A and B, of this paper and Figure 2F of the accompanying paper [Clarke *et al.,* 2020]). We propose that this is useful and probably essential for responding accurately to the shallow, often noisy gradients of individual guidance cues, which are typically presented in complex combinations. In this sense, the mechanism we have found is most akin to the mechanism of bacterial chemotaxis, in which external attractants and repellants provide only a subtle spatial bias to essentially stochastic fluctuations of the motility machinery, relying on a "random walk with a ratchet" to produce net guidance (Macnab and Koshland, 1972; Wadhams and Armitage, 2004). A corollary to this, of course, is that no single time point determines future development. Even in wild type, the actin peak can and often does transiently fragment, recede, or invade nonpreferred projections before eventually converging on the genetically designated trajectory. Additionally, we note that these actin fluctuations survey all growth cone protrusions—off-axis lateral projections as well as on-axis extensions of the axon shaft—thereby allowing growth cone turning to derive from the same machinery as does linear extension of the axon.

The wave-like, anterograde propagation of an actin distribution, which is regulated by the conserved Abl tyrosine kinase and which probabilistically localizes the site of filopodial dynamics, represents a novel mechanism of motility that drives the extension and guidance of TSM1 in the intact *Drosophila* wing. This style of growth expands our understanding of the fundamental mechanisms used by neurons to build neural circuits and reveals a novel molecular and cellular mechanism for Abl, one of the central regulators of cell morphology and neural wiring.

MATERIALS AND METHODS

Drosophila stocks

Drosophila stocks are the same as for the accompanying paper (Clarke *et al.,* 2020).

Imaging methods, data extraction, and image data set

All methods of imaging, image segmentation and tracing, and data extraction were the same as for the accompanying paper (Clarke *et al.*, 2020). The wild-type, Abl KD, and Abl OE data sets were the same as those used in the accompanying paper (Clarke *et al.*, 2020).

Quantification of protrusions in response to actin distribution translocation

To quantify the effect that actin advance has on local axonal protrusion, we summed the length of protrusions in a 10-µm interval surrounding the midpoint of the actin distribution at the start of a 20-µm translocation and in a 10-µm interval surrounding the endpoint of the translocation (MATLAB).

Pharmacology: actin disruption by LatB

LatB suspended in DMSO was added to 5 ml of culture media for a final concentration of 10 µM LatB/0.1% DMSO in explant wing cultures 5 min before imaging. Cultures were imaged as described in the accompanying paper (Clarke *et al.*, 2020).

Wavelet analysis of actin distributions

The Daubechies type 4 (D4) wavelet transformation, modified to properly account for the profile boundaries, was used to extract and quantify the intrinsic frequency components of the actin distributions according to the formulas

$$S_{2,n} = \sum_{m=1}^{4} c_m \, S_{1,2n+m-2}$$

$$D_{2,n} = \sum_{m=1}^{4} d_m S_{1,2n+m-2}$$

where NB = the binned actin intensity profile, $n = 1, 2, \ldots NB/4$, c_m specifies the low pass filter components, and d_m specifies the high pass filter components. For each actin distribution intensity profile, the intensity data were binned in one of two ways: 1) $NB = 512$ with bin width = 0.25 µm and 2) $NB = 2048$ with bin width = 0.06 µm. For each distribution, bins overlapping the end of the axon were padded with zero to prevent edge effects.

Statistics, reproducibility, and data and code availability

Statistics, reproducibility, and code availability are as described for the accompanying paper (Clarke *et al.*, 2020). In brief, all statistical tests and their respective parameters are reported in the text and figure legends. Sample randomization was not relevant. In-focus samples were excluded only if the absolute intensity of fluorescent signal was too low for quantification or if at the time of initiating imaging 1) there was no axon visible in the vicinity of the normal trajectory, or 2) the axon showed no evidence of dynamics (i.e., the

cell seemed dead). Trajectories were terminated if the TSM1 growth cone went out of the plane of focus or fasciculated with the L3 nerve, or after 90 min of imaging. Blinding was not relevant as all analyses were done with a computational pipeline. No formal power analysis was done to determine sample size prior to initiating experiment; retrospective leave-out analyses demonstrated that all reported observations were robust to final sample size. Numerical data for all figures are included in Supplemental Datasheet 1. MiPav plug-in code for extraction of actin intensity profiles has been incorporated and released in the publicly available National Institutes of Health (NIH) image analysis package package, MiPav. MATLAB and Mathematica scripts are available on the publicly accessible NIH website: https://data.ninds.nih.gov/EGiniger/clarke/index.html.

ACKNOWLEDGMENTS

We thank all the members of our lab for their advice and assistance during the course of these experiments, particularly Kate O'Neill for MATLAB expertise. We also particularly thank Chi-Hon Lee, Sally Moody, Clare Waterman, Bob Fischer, Chun-Yuan Ting, Lenny Campanello, Wolfgang Losert, and Garyk Papoian for their many helpful suggestions and Laura Alto, Jon Terman, and Ken Yamada for comments on the manuscript. Additionally, we thank Mike Murrell and Ian Linsmeier for sharing their data and ideas about the motions of actin molecules and Valerie Castellani for sharing unpublished data on fine-scale localization of guidance receptors in the growth cone. Many *Drosophila* stocks were provided by the Bloomington *Drosophila* Stock Center. This work utilized the computational resources of the NIH High Performing Computation Biowulf cluster (http://hpc.nih.gov) and the Cytogenetics and Microscopy Core Facility of the National Human Genome Research Institute (NHGRI). These experiments were supported in part by the Basic Neuroscience Program of the National Institute of Neurological Disorders and Stroke Intramural Research Program (Z01-NS003013 to E.G.). P.G.M., V.W., and E.McC. were supported by the Intramural Research Program of NIH, Center for Informational Technology, and S.W. was supported by the NHGRI, NIH. R.K. was supported in part by a DBT Ramalingaswami reentry fellowship from the Government of India.

REFERENCES

Bagonis MM, Fusco L, Pertz O, Danuser G (2019). Automated profiling of growth cone heterogeneity defines relations between morphology and motility. J Cell Biol 218, 350–379.

Bilancia CG, Winkelman JD, Tsygankov D, Nowotarski SH, Sees JA, Comber K, Evans I, Lakhani V, Wood W, Elston TC, *et al.* (2014). Enabled negatively regulates diaphanous-driven actin dynamics in vitro and in vivo. Dev Cell 28, 394–408.

Clarke A, McQueen PG, Fang HY, Kannan R, Wang V, McCreedy E, Buckley T, Johannessen EM, Wincovitch S, Giniger E (2020). Dynamic morphogenesis of a pioneer axon in *Drosophila* and its regulation by Abl tyrosine kinase. Mol Biol Cell 31, XXX–XXX.

Cohen M, Georgiou M, Stevenson NL, Miodownik M, Baum B (2010). Dynamic filopodia transmit intermittent Delta-Notch signaling to drive pattern refinement during lateral inhibition. Dev Cell 19, 78–89.

Crowner D, Le Gall M, Gates MA, Giniger E (2003). Notch steers Drosophila ISNb motor axons by regulating the Abl signaling pathway. Curr Biol 13, 967–972.

Dent EW, Gertler FB (2003). Cytoskeletal dynamics and transport in growth cone motility and axon guidance. Neuron 40, 209–227.

Ennomani H, Letort G, Guerin C, Martiel JL, Cao W, Nedelec F, De La Cruz EM, Thery M, Blanchoin L (2016). Architecture and connectivity govern actin network contractility. Curr Biol 26, 616–626.

Forsthoefel DJ, Liebl EC, Kolodziej PA, Seeger MA (2005). The Abelson tyrosine kinase, the trio GEF and enabled interact with the netrin receptor frazzled in Drosophila. Development 132, 1983–1994.

Goncalves-Pimentel C, Gombos R, Mihaly J, Sanchez-Soriano N, Prokop A (2011). Dissecting regulatory networks of filopodia formation in a Drosophila growth cone model. PLoS One 6, e18340.

Grevengoed EE, Fox DT, Gates J, Peifer M (2003). Balancing different types of actin polymerization at distinct sites: roles for Abelson kinase and Enabled. J Cell Biol 163, 1267–1279.

Grevengoed EE, Loureiro JJ, Jesse TL, Peifer M (2001). Abelson kinase regulates epithelial morphogenesis in Drosophila. J Cell Biol 155, 1185–1198.

He L, Wang X, Tang HL, Montell DJ (2010). Tissue elongation requires oscillating contractions of a basal actomyosin network. Nat Cell Biol 12, 1133–1142.

Kannan R, Cox E, Wang L, Kuzina I, Gu Q, Giniger E (2018). Tyrosine phosphorylation and proteolytic cleavage of Notch are required for non-canonical Notch/Abl signaling in Drosophila axon guidance. Development 145, dev151548.

Kannan R, Song JK, Karpova T, Clarke A, Shivalkar M, Wang B, Kotlyanskaya L, Kuzina I, Gu Q, Giniger E (2017). The Abl pathway bifurcates to balance Enabled and Rac signaling in axon patterning in Drosophila. Development 144, 487–498.

Koleske AJ, Gifford AM, Scott ML, Nee M, Bronson RT, Miczek KA, Baltimore D (1998). Essential roles for the Abl and Arg tyrosine kinases in neurulation. Neuron 21, 1259–1272.

Kulkarni G, Xu Z, Mohamed AM, Li H, Tang X, Limerick G, Wadsworth WG (2013). Experimental evidence for UNC-6 (netrin) axon guidance by stochastic fluctuations of intracellular UNC-40 (DCC) outgrowth activity. Biol Open 2, 1300–1312.

Kuzina I, Song JK, Giniger E (2011). How Notch establishes longitudinal axon connections between successive segments of the Drosophila CNS. Development 138, 1839–1849.

Lebrand C, Dent EW, Strasser GA, Lanier LM, Krause M, Svitkina TM, Borisy GG, Gertler FB (2004). Critical role of Ena/VASP proteins for filopodia formation in neurons and in function downstream of netrin-1. Neuron 42, 37–49.

Lee H, Engel U, Rusch J, Scherrer S, Sheard K, Van Vactor D (2004). The microtubule plus end tracking protein Orbit/MAST/CLASP acts downstream of the tyrosine kinase Abl in mediating axon guidance. Neuron 42, 913–926.

Lenz M (2014). Geometrical origins of contractility in disordered actomyosin networks. Phys Rev X 4, 041002.

Lewis AK, Bridgman PC (1992). Nerve growth cone lamellipodia contain two populations of actin filaments that differ in organization and polarity. J Cell Biol 119, 1219–1243.

Liebl EC, Rowe RG, Forsthoefel DJ, Stammler AL, Schmidt ER, Turski M, Seeger MA (2003). Interactions between the secreted protein Amalgam, its transmembrane receptor Neurotactin and the Abelson tyrosine kinase affect axon pathfinding. Development 130, 3217–3226.

Lin CH, Forscher P (1995). Growth cone advance is inversely proportional to retrograde F-actin flow. Neuron 14, 763–771.

Linsmeier I, Banerjee S, Oakes PW, Jung W, Kim T, Murrell MP (2016). Disordered actomyosin networks are sufficient to produce cooperative and telescopic contractility. Nat Commun 7, 12615.

Lowery LA, Van Vactor D (2009). The trip of the tip: understanding the growth cone machinery. Nat Rev Mol Cell Biol 10, 332–343.

Macnab RM, Koshland DE Jr (1972). The gradient-sensing mechanism in bacterial chemotaxis. Proc Natl Acad Sci USA 69, 2509–2512.

Mogilner A, Rubinstein B (2005). The physics of filopodial protrusion. Biophys J 89, 782–795.

Moresco EM, Koleske AJ (2003). Regulation of neuronal morphogenesis and synaptic function by Abl family kinases. Curr Opin Neurobiol 13, 535–544.

O'Connor TP, Duerr JS, Bentley D (1990). Pioneer growth cone steering decisions mediated by single filopodial contacts in situ. J Neurosci 10, 3935–3946.

O'Donnell MP, Bashaw GJ (2013). Distinct functional domains of the Abelson tyrosine kinase control axon guidance responses to Netrin and Slit to regulate the assembly of neural circuits. Development 140, 2724–2733.

Padmanabhan P, Goodhill GJ (2018). Axon growth regulation by a bistable molecular switch. Proc Biol Sci 285.

Pignata A, Ducuing H, Boubakar L, Gardette T, Kindbeiter K, Bozon M, Tauszig-Delamasure S, Falk J, Thoumine O, Castellani V (2019). A spatiotemporal sequence of sensitization to slits and semaphorins orchestrates commissural axon navigation. Cell Rep 29, 347–362.e345.

Sabry JH, O'Connor TP, Evans L, Toroian-Raymond A, Kirschner M, Bentley D (1991). Microtubule behavior during guidance of pioneer neuron growth cones in situ. J Cell Biol 115, 381–395.

Sanchez-Soriano N, Goncalves-Pimentel C, Beaven R, Haessler U, Ofner-Ziegenfuss L, Ballestrem C, Prokop A (2010). Drosophila growth

cones: a genetically tractable platform for the analysis of axonal growth dynamics. Dev Neurobiol 70, 58–71.
Suter DM, Forscher P (2000). Substrate-cytoskeletal coupling as a mechanism for the regulation of growth cone motility and guidance. J Neurobiol 44, 97–113.
Svitkina TM, Bulanova EA, Chaga OY, Vignjevic DM, Kojima S, Vasiliev JM, Borisy GG (2003). Mechanism of filopodia initiation by reorganization of a dendritic network. J Cell Biol 160, 409–421.
Wadhams GH, Armitage JP (2004). Making sense of it all: bacterial chemotaxis. Nat Rev Mol Cell Biol 5, 1024–1037.
Wills Z, Bateman J, Korey CA, Comer A, Van Vactor D (1999a). The tyrosine kinase Abl and its substrate enabled collaborate with the receptor phosphatase Dlar to control motor axon guidance. Neuron 22, 301–312.
Wills Z, Marr L, Zinn K, Goodman CS, Van Vactor D (1999b). Profilin and the Abl tyrosine kinase are required for motor axon outgrowth in the Drosophila embryo. Neuron 22, 291–299.